

STEAM TURBINE MATERIALS AND CORROSION

Gordon R. Holcomb
NETL-Albany, 1450 Queen Ave SW, Albany, OR 97321
Email: Gordon.Holcomb@netl.doe.gov; Voice: (541) 967-5874; Fax: (541)-967-5914

David E. Alman
NETL-Albany, 1450 Queen Ave SW, Albany, OR 97321
Email: David.Alman@netl.doe.gov; Voice: (541) 967-5885; Fax: (541)-967-5845

Ömer N. Doğan
NETL-Albany, 1450 Queen Ave SW, Albany, OR 97321
Email: Omer.Dogan@netl.doe.gov; Voice: (541) 967-5858; Fax: (541)-967-5845

James C. Rawers
NETL-Albany, 1450 Queen Ave SW, Albany, OR 97321
Email: James.Rawers@netl.doe.gov; Voice: (541) 967-5882; Fax: (541)-967-5845

Karol K. Schrems
NETL-Albany, 1450 Queen Ave SW, Albany, OR 97321
Email: Karol.Schrems@netl.doe.gov; Voice: (541) 967-5804; Fax: (541)-967-5845

Malgorzata Ziomek-Moroz
NETL-Albany, 1450 Queen Ave SW, Albany, OR 97321
Email: Margaret.Ziomek-Moroz@netl.doe.gov; Voice: (541) 967-5943; Fax: (541)-967-5914

ABSTRACT

Ultra-supercritical (USC) power plants offer the promise of higher efficiencies and lower emissions. Current goals of the U.S. Department of Energy's Advanced Power Systems Initiatives include power generation from coal at 60% efficiency, which would require steam temperatures of up to 760°C. This project examines the steamside oxidation of candidate alloys for use in USC systems, with emphasis placed on applications in high- and intermediate-pressure turbines. As part of this research a concern has arisen about the possibility of high chromia evaporation rates of protective scales in the turbine. A model to calculate chromia evaporation rates is presented.

INTRODUCTION

Current goals of the U.S. Department of Energy's Advanced Power Systems Initiatives include power generation from coal at 60% efficiency, which would require steam conditions of up to 760°C and 35MPa, so called ultra-supercritical (USC) steam conditions. This is in comparison to conventional sub-critical steam plants which operate at about 37% efficiency (steam at 540°C-14.5 MPa) and advanced plants that are currently just being introduced into the market that operate at 40 to 45% efficiency (steam at 600°C-28MPa). The importance of increased efficiency is because it is estimated that for each 1% raise in plant efficiency will eliminate approximately 1,000,000 tons of CO₂ over the lifetime of an 800MW coal fired plant.¹ The overarching limitation to achieving the DOE goal is a lack of cost effective metallic

materials that can perform at these temperatures and pressures.² Improving alloy resistance to high temperature corrosion is one key in developing new, efficient and clean coal-fired ultra-supercritical (USC) steam plants.²

For the USC application, both turbine and boiler materials will operate at higher temperatures and pressures than in conventional plants. However, the development of creep strength in alloys is often obtained at the expense of corrosion and oxidation resistance. Therefore, the strategies to confer corrosion resistance may be needed if ever increasing cycle temperatures are to be achieved in advanced plants. To identify or develop alloys and strategies that can meet these performance requirements, it is critical to understand the degradation mechanisms that will occur during operation.

A critical aspect of materials usage in USC steam turbines is oxidation behavior. Oxidation can result in several adverse conditions: general section loss from material thinning, deep and localized section loss from internal oxidation along grain boundaries, dimensional changes that are critical in airfoils, and downstream erosion from oxide spallation. Evaporation of protective chromia scales may also be an issue at the higher temperatures and pressures of USC steam turbines. In addition, oxidation may modify creep behavior (beyond mere section loss) by its near-surface effects on grain boundary morphologies and precipitation strengthening.

PROJECT OBJECTIVES

The objective of this research is to understand materials degradation in USC steam environments and to identify and/or develop viable materials for use in USC steam turbines. A variety of materials-based approaches are used that can be broadly categorized into steam oxidation, surface treatments, and alloy development. The steam oxidation portion of this research is presented here.

There are two basic objectives of the steam oxidation research. The first is to characterize candidate commercial alloys (primarily nickel-base superalloys) as to their steam oxidation resistance. An important consideration in this was to compliment, and not to duplicate, other DOE-sponsored research in this arena—namely the USC boiler consortium effort in atmospheric pressure steam.

The second objective is to develop steam oxidation models for use in USC steam turbine environments. Thus far modeling has focused on chromia evaporation. Future plans include the development of models to address geometric effects on oxide spallation, and high temperature creep and oxidation interactions.

OXIDATION BEHAVIOR OF CANDIDATE ALLOYS

The oxidation behavior is examined of candidate alloys for use in USC steam turbines. Alloys include the most promising alloys identified by the USC boiler and turbine consortiums, the UK-US Collaboration on Energy Research & Development in the Field of Fossil Energy Technology, the Electric Power Research Institute (EPRI),³ and in use in the Scholven Unit F demonstration.⁴ These are listed in Table 1. The USC turbine consortium alloys (Udimet 720, Haynes 282, and Nimonic 105) were recently obtained from GE-Energy (Schenectady, NY) and added to the study.

Table 1. Candidate alloys for use in advanced steam turbines.

Alloy	Class	USC Boiler	EPRI Turbine Candidate	Scholven Unit F Turbine	UK-US	USC Turbine
T92	Fe Ferritic	X			RR	
SAVE12 9.5Cr	Fe Ferritic	X			X	
SAVE12 10.5Cr	Fe Ferritic	X			X	
TP347HFG	Fe Austenitic	X			RR	
HR6W	High Ni & Cr	X				
Haynes 230	Ni Superalloy	X			X	
Haynes 282	Ni Superalloy					X
Inconel 617	Ni Superalloy	X		X	X	
Inconel 625	Ni Superalloy			X	X	
Inconel 718	Ni Superalloy		X		X	
Inconel 740	Ni Superalloy	X			RR	
Nimonic 90	Ni Superalloy		X		X	
Nimonic 105	Ni Superalloy					X
Udimet 720Li	Ni Superalloy					X

Current tests are at ambient pressures and include furnace exposures, thermogravimetric analysis (TGA), and cyclic oxidation. These test procedures were earlier described in detail.⁵ In brief, furnace exposures were for up to 2000 hr in air with 3% water vapor with 100 hour temperature cycles and slow heating and cooling rates. TGA tests were for 300 hr in Ar with 35% water vapor. Cyclic oxidation tests were for up to 2000 cycles in air with 40% water vapor with hourly temperature cycles with rapid heating and cooling rates. Progress in the testing plan is shown in Table 2.

Table 2. Percentage of completed tests for each alloy at each temperature.

Alloy	°C	Cyclic				Furnace				TGA			
		650	700	760	800	650	700	760	800	650	700	760	800
T92		0%	0%	100%		100%	36%	100%	71%	0%	0%	0%	0%
Save12 9.5 Cr		41%	0%	100%		100%	54%	100%	36%	0%	0%	75%	100%
Save12 10.5 Cr		41%	0%	100%		100%	54%	100%	36%	0%	0%	75%	100%
TP347HFG		0%	0%	100%	0%	100%	36%	100%	71%	0%	0%	0%	0%
HR6W		0%	0%	100%	0%	100%	36%	100%	71%				50%
Haynes 230		0%	0%	100%	0%	100%	41%	100%	36%				100%
Inconel 617		0%	0%	100%	0%	100%	36%	100%	36%				100%
Inconel 625		0%	0%	100%	0%	100%	71%	100%	71%				50%
Inconel 718		0%	0%	100%	0%	100%	0%	100%	36%				0%
Inconel 740		0%	0%	100%	0%	100%	54%	100%	36%				25%
Nimonic 90		0%	0%	100%	0%	100%	36%	100%	36%				0%

As examples of the kinetics and microstructures found, representative results from cyclic oxidation tests are shown in Figs. 1-4 at 760°C for Inconel 740, Haynes 230, Inconel 718, and Nimonic 90. Of note are the decreases in mass with time for Haynes 230, Inconel 718, and to a lesser extent, Inconel 740. No spalling was observed, so this decrease indicates evaporative losses. Scale thickness with time is a competition between scale growth from oxidation and scale loss from evaporation. Nimonic 90, with its higher oxidation rate and thicker scale did not yet show the gradual decrease in mass with time that indicates a steady state scale thickness has been reached. The microstructures shown in Figs. 1-4 show that internal oxidation of aluminum has occurred beneath the oxide scale and predominantly along grain boundaries.

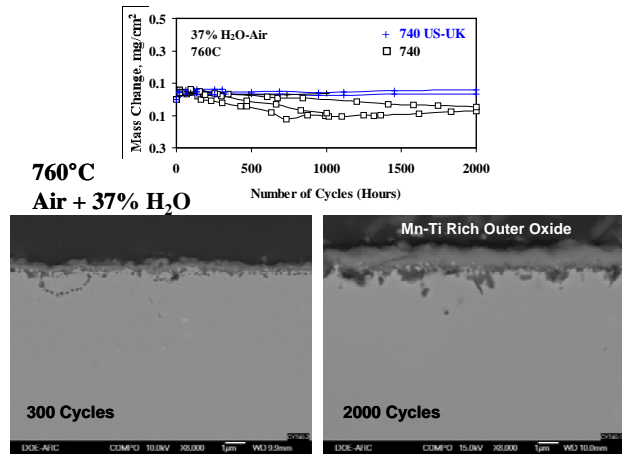


Fig. 1. Cyclic oxidation of Inconel 740 at 760°C.

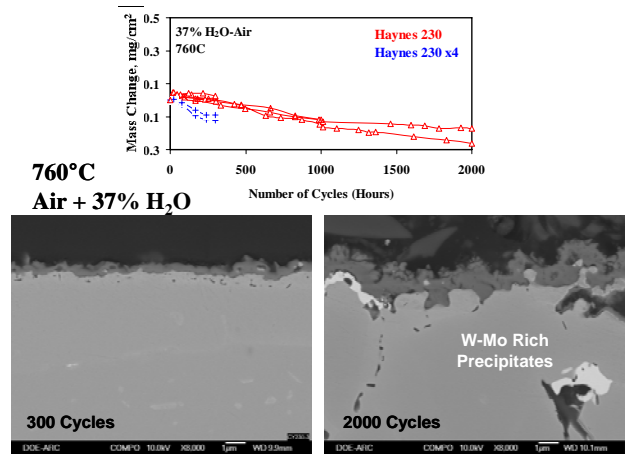


Fig. 2. Cyclic oxidation of Haynes 230 at 760°C.

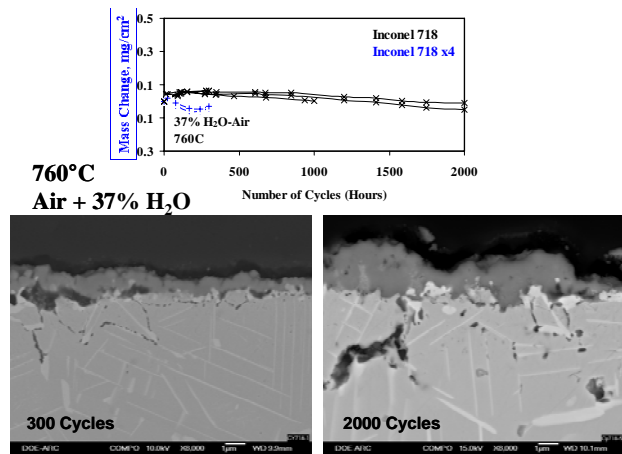


Fig. 3. Cyclic oxidation of Inconel 718 at 760°C.

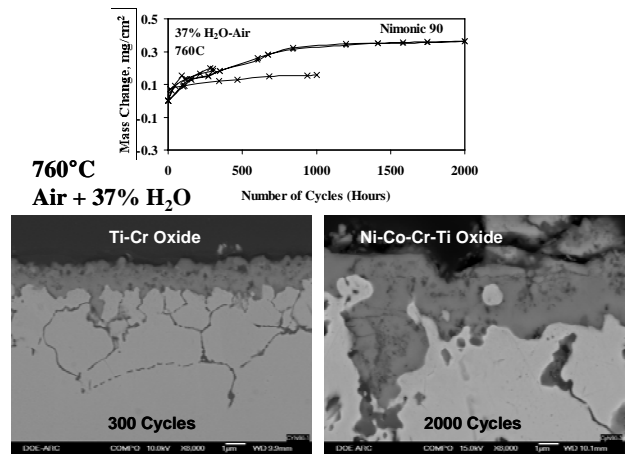
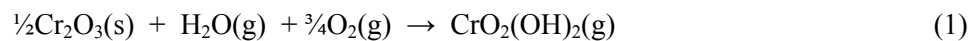


Fig. 4. Cyclic oxidation of Nimonic 90 at 760°C.

In contrast with cyclic tests, furnace exposures show mass increases with time. Chromia evaporation is suppressed in these furnace exposures due to 1) the samples being in crucibles and thus less exposed to the flowing gas, and 2) a much lower water vapor partial pressure.

CHROMIA EVAPORATION MODEL

The oxidation of alloys protected by the formation of Cr_2O_3 (chromia formers) can undergo scale loss due to reactive evaporation of chromium containing gas species. Water vapor increases the evaporation loss by allowing the formation of $\text{CrO}_2(\text{OH})_2(\text{g})$, which has a higher vapor pressure than $\text{CrO}_3(\text{g})$. $\text{CrO}_3(\text{g})$ is the predominate Cr gas specie in dry air or oxygen. The reaction is given by Eq. (1).



Evaporation can change the overall oxidation kinetics from parabolic behavior to linear kinetics or even to breakaway oxidation. Linear kinetics can arise after scale growth from oxidation, which decreases with increasing scale thickness, matches the scale loss from reactive evaporation. The change in scale thickness, x , with time, t can be described in terms of the parabolic rate constant, k_p , and the linear reactive evaporation rate, k_e , as:

$$\frac{dx}{dt} = \frac{k_p}{x} - k_e \quad (2)$$

At long times or high reactive evaporation rates, a limiting scale thickness, x_L , arises that is given by:

$$x_L = \frac{k_p}{k_e} \quad (3)$$

The approach used to determine evaporation rates was to assume that volatility is limited by the transport of $\text{CrO}_2(\text{OH})_2(\text{g})$ through a boundary layer in the gas phase. For flat plate geometry with laminar flow, the evaporation rate can be calculated by:⁶⁻⁷

$$k_e \left(\frac{\text{kg}}{\text{m}^2 \cdot \text{s}} \right) = 0.664 Re^{0.5} Sc^{0.343} \frac{D_{AB} \rho}{L} \quad (4)$$

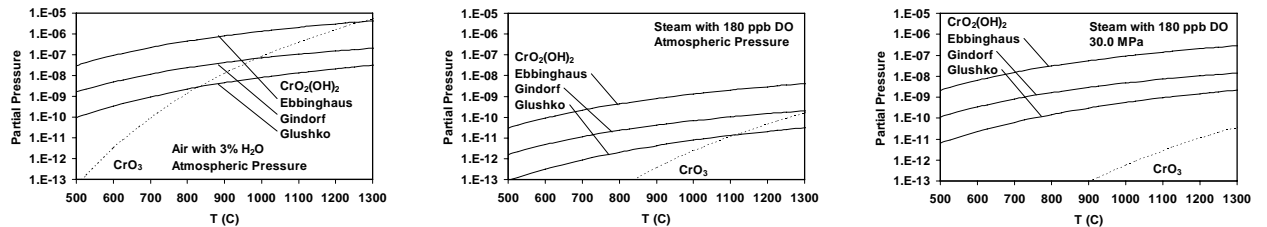
Where Re and Sc are the dimensionless Reynolds and Schmidt numbers, D_{AB} is the gaseous diffusion coefficient between the Cr gas specie and the solvent gas (m^2/s), ρ is the density (kg/m^3) of the evaporative specie in the gas, and L is the length (m) in the flow direction of the flat plate. Equation 4 is valid for Sc numbers between 0.6 and 50.⁶ Assuming ideal gas behavior and a reaction described by Eq. (1), this can be expanded to:

$$k_e \left(\frac{\text{kg}}{\text{m}^2 \cdot \text{s}} \right) = 0.664 Re^{0.5} Sc^{0.343} \frac{D_{AB} M_i P_T}{LRT} P_{\text{H}_2\text{O}} P_{\text{O}_2}^{3/4} \exp\left(-\frac{\Delta G}{RT}\right) \quad (5)$$

Where M_i is the molecular mass of $\text{CrO}_2(\text{OH})_2(\text{g})$, P_T is the total pressure, ΔG is the Gibbs energy of Eq. (1), and $P_{\text{H}_2\text{O}}$ and P_{O_2} are partial pressures of H_2O and O_2 . In a similar fashion for turbulent flow ($Re > 5 \times 10^5$):

$$k_e \left(\frac{\text{kg}}{\text{m}^2 \cdot \text{s}} \right) = 0.0592 Re^{4/5} Sc^{1/3} \frac{D_{AB} M_i P_T}{LRT} P_{\text{H}_2\text{O}} P_{\text{O}_2}^{3/4} \exp\left(-\frac{\Delta G}{RT}\right) \quad (6)$$

The right-hand sides of Eqs. (5-6) are essentially the partial pressure of $\text{CrO}_2(\text{OH})_2(\text{g})$, which depends on ΔG . Figure 5 shows the dependence of $P_{\text{CrO}_2(\text{OH})_2}$ from T , P_T , and three literature sources for ΔG .⁸⁻¹⁰ The P_{O_2} dependence lowers $P_{\text{CrO}_2(\text{OH})_2}$ going from moist air to oxygenated steam, while increasing the total pressure lowers ΔG and increases $P_{\text{CrO}_2(\text{OH})_2}$.



a) b) c)
Fig. 5. Partial pressures over pure Cr_2O_3 for a) 3% H_2O in air at atmospheric pressure, b) steam with 180 ppb dissolved oxygen (DO) at atmospheric pressure, and c) steam with 180 ppb DO at 30.0 MPa. The three curves for $\text{CrO}_2(\text{OH})_2(\text{g})$ arise from three literature sources for ΔG .⁸⁻¹⁰

The cyclic oxidation tests were done with gas flowing parallel to the flat sample surface, and so can be described by Eq. (5). Figure 6 shows mass change results from Haynes 230 at 760°C for two different gas velocities compared with predicted evaporation mass loss. The agreement is excellent using the Gindorf¹⁰ values for ΔG .

The model was applied to steam turbine conditions using Eq. (6). Some predictions are shown in Fig. 7 for supercritical steam with 180 ppb dissolved oxygen (DO). These predicted rates are quite large compared to the experimental tests at atmospheric pressure and low gas velocities. The highest value in Fig. 7 (for 760°C and 34.5 MPa) of 3.84×10^{-7} kg/m²/s corresponds to about 0.6 mm per year of metal loss (assumes a metal density of 9 g/cm³ and a conversion to a Cr basis). This is a large value for metal loss for a component expected to operate many years, and it may be larger if the scale losses enough Cr to become non-protective. Current state-of-the-art steam turbines operate at approximately 600°C and 30 MPa, and would have a predicted evaporation rate of about 8×10^{-8} kg/m²/s. Typical subcritical steam power plants operate at 538°C and 16.5 MPa, and would have a predicted evaporation rate of about 2×10^{-8} kg/m²/s. These later two cases should have lower evaporation rates in practice because the ferritic-martensitic steels used usually form Fe-Cr spinel outer scales instead of chromia scales. This lowers the activity of chromia in the scale, which lowers the partial pressure of CrO₂(OH)₂(g) and thus lower the evaporation rate.

Another factor that would lower the predicted evaporation rate for USC conditions is that the gas is assumed to be free of already existing CrO₂(OH)₂(g). But the superheater, with a steam velocity of 10-25 m/s, undoubtedly undergoes significant evaporative attack that would partially saturate the gas entering the turbine. This could shift the most damaging attack from the turbine to the superheater.

Laboratory corrosion tests generally seek to mimic the process environment as closely as possible. In cases where this is difficult, then one seeks to establish conditions where the corrosion mechanisms are the same. For steam turbines, laboratory tests with the same combination of temperature, pressure, gas velocities, and steam chemistry are extremely difficult and expensive. Therefore tests sacrifice one or more of the conditions—usually pressure or gas velocity. For examining the effects of Cr-evaporation as a corrosion mechanism, laboratory tests may be best served with much higher oxygen partial pressures so as to increase the evaporation rate. In Fig. 8 the advanced steam turbine points are from the 760°C data Fig. 6. The representative laboratory curves are as a function of the partial pressure of O₂ in Air+H₂O and O₂+H₂O atmospheres. The laboratory curves were all calculated at atmospheric pressure, $v = 0.02$ m/s and $L = 0.02$ m. The right-hand-side of the laboratory curves drop sharply as P_{H_2O} approaches zero. The right-hand-side end points of the laboratory curves are limits—reactive evaporation in drier O₂ or drier air would switch at that point from CrO₂(OH)₂(g) being the dominate gas specie to CrO₃(g), and would not drop further with less H₂O.

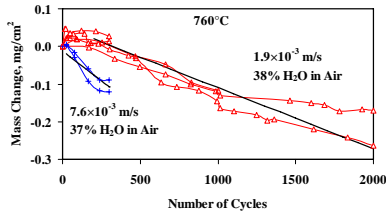


Fig. 6. Cyclic oxidation of Haynes 230 at 760°C. Straight solid lines are the predicted slopes from reactive evaporation of $\text{Cr}_2\text{O}_3(\text{s})$ using the Gindorf¹⁰ data for $\text{CrO}_2(\text{OH})_2(\text{g})$.

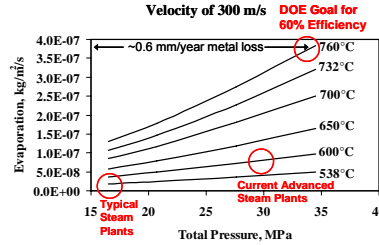


Fig. 7. Predicted evaporation rates in steam with 180 ppb DO, 300 m/s flow rate, and a characteristic length of 0.05 m.

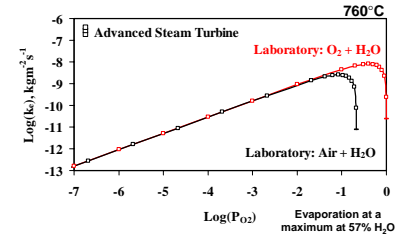


Fig. 8. Predicted evaporation rates at 760°C for USC turbines (180 ppb DO, P_T of 20.7, 27.5 and 34.5 MPa, $v = 300$ m/s) compared with atmospheric pressure laboratory tests.

NEAR TERM FUTURE WORK

From the start of this project, a goal has been to examine the effects of pressure on steam oxidation. Procurement of the main component required for USC steam exposures, the autoclave, took over three years of solicitations, cancellations, and renegotiations. The autoclave arrived in December of 2006 and is currently being brought on-line. It is of Haynes 230 construction and is dual rated for temperatures and pressures of up to either 4500 psi at 1400°F (310 bar at 760°C) or 5000 psi at 1375°F (345 bar at 746°C). Some photographs of it are in Fig. 9. A schematic of the entire setup is in Fig. 10. Comparisons between field and autoclave exposures to supercritical steam are planned.



Fig. 9. The Haynes 230 autoclave dual rated for temperatures and pressures of up to either 310 bar at 760°C or 345 bar at 746°C.

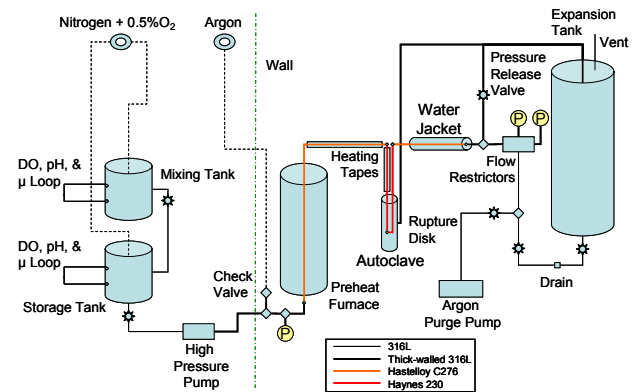


Fig. 10. Schematic of the USC exposure apparatus.

Also planned are studies on the geometric effects on oxide spallation by examining the oxidation of wires of differing diameters, and on interactions between oxidation and creep behavior.

SUMMARY

Steam oxidation behavior is directly linked to implementing USC steam power generation for improved efficiencies and reduced CO₂ emissions. Two basic objectives of the steam oxidation research were presented. The first was to characterize candidate commercial alloys (primarily nickel-base superalloys) as to their steam oxidation resistance. Beyond simple scale formation, the primary degradation mechanisms were shown to be internal oxidation and chromia evaporation. The second objective was to develop steam oxidation models for use in USC steam turbine environments. A model was shown for chromia evaporation and predictions were made as far as extending the model to USC conditions.

REFERENCES

1. R. Swanekamp, *Power*, 146 (4), 2002, pp. 32-40.
2. R. Viswanathan, J. F. Henry, J. Tanzosh, G. Stanko, J. Shingledecker, B. Vitalis, R. Purgert, *Journal of Materials Engineering and Performance*, 14, 2005, pp. 281-292.
3. R. Viswanathan and W. Bakker, *Journal of Materials Engineering and Performance*, 10, 2001, pp. 96-101.
4. "Materials Development in the European AD700 Program," *Materials & Components in Fossil Energy Applications*, No. 162, Spring/Summer 2005, U.S. Department of Energy.
5. G. R. Holcomb and M. Ziomek-Moroz, "Steam Turbine Materials and Corrosion," *Proceedings of the 20th Annual Conference on Fossil Energy Materials*, Knoxville, TN, June 12-14, 2006 (U.S. Department of Energy, Office of Fossil Energy, Advanced Research Materials).
6. D. R. Gaskell, *An Introduction to Transport Phenomena*, New York (NY): Macmillan Publishing, 1992, pp. 78-89 (chapter 2) and 569-578 (chapter 11).
7. G. H. Geiger, D. R. Poirier, *Transport Phenomena in Metallurgy*, Reading (MA): Addison-Wesley Publishing, 1973, pp. 7-13 (chapter 1), 463-467 (chapter 13) and 529-537 (chapter 15).
8. Glusko Thermocenter of the Russian Academy of Sciences—Izhorskaya 13/19, 127412, Moscow Russia: IVTAN Association; 1994.
9. B. B. Ebbinghaus, *Combustion and Flame*, Vol. 93, 1993, pp. 119-137.
10. C. Gindorf, K. Hilpert, L. Singheiser, "Determination of Chromium Vaporization Rates of Different Interconnect Alloys by Transpiration Experiments. H. Yokokawa, S. C. Singhal, editors, in Solid Oxide Fuel Cells (SOFC VII), Proceedings Vol. 2001-16, Pennington (NJ): Electrochemical Society, 2001, pp. 793-802.